Low-Frequency-Drop of Electroabsorption Modulated Lasers and the Improvement With Partially Corrugated Grating Based DFB Lasers

Siti Sulikhah, *Member, IEEE*, San-Liang Lee, *Senior Member, IEEE*, Lung-Wei Chung, and Hen-Wai Tsao, *Senior Member, IEEE*

***Abstract*—Electroabsorption modulated lasers (EMLs) is sensitive to the residual facet reflection (RFR), which can cause a low-frequency drop (LFD) in the modulation response. The LFD may result in output waveform distortion, especially for high-data rate and multi-level modulation. We verify by simulation and experiments that the effect of LFD on the EML performance and propose to use LFD as one of the key performance indices for qualifying EMLs in high-speed optical transceivers. LFD can be suppressed by incorporating partial-corrugated-grating (PCG) in the laser section. With PCG-DFB structure, the EMLs can maintain high single-mode yield (SMY) and an excellent quality factor even with a strong modulator reflection from EAM section. This provides the robustness in applying the PCG-DFB to achieve a flat intensity modulation response or to enhance the output waveform under large signal modulation. By designing the PCG-EML to have about 60% of grating region, it can reach >80% of SMY and improve the average Q-value from the reduced LFD in the modulation response. The PCG-EML with reduced LFD can enhance the eye-opening through reduced waveform undershoot and overshoot for transmitting 56-Gbaud/s or beyond PAM-4 signals.**

***Index Terms*—Electroabsorption, low-frequency drop, optical communication, partial grating, residual facet reflection.**

I. Introduction

THE rapid expansion of cloud computing, big data, and applications with smart mobile devices, intra- and inter-data center traffics are growing remarkably with the extension of next-generation high-speed light sources and 5G mobile network technology. The emerging IEEE 802.3ck standard for 800GbE or 1.6TbE has started to be discussed [1]. Currently, 4-level pulse amplitude modulation (PAM-4) has been standardized for these applications as it allows to doubling the actual data rate compared with conventional non-return-to-zero (NRZ) modulation. The current electroabsorption modulated lasers (EMLs) can provide enough bandwidth to carry 100-Gb/s and above per channel data rate for optical interconnect applications. EMLs are very enticing due to their compactness, low packaging cost, low chirp, robustness, low driving voltage, high extinction ratio, high stability, and large modulation bandwidth [2], [3]. The preliminary guideline for EMLs to support 200-Gb/s per lane are having a high bandwidth of 42-GHz to 55-GHz from the integrated electroabsorption modulator (EAM) and the use of PAM-4 or PAM-6 formats [4]. Recently, the uncooled 53-Gbaud/s PAM-4 operation using an InGaAsP-MQW EML was demonstrated with a low driving voltage of 0.9-*V* peak-to-peak voltage (*Vpp*) [5].

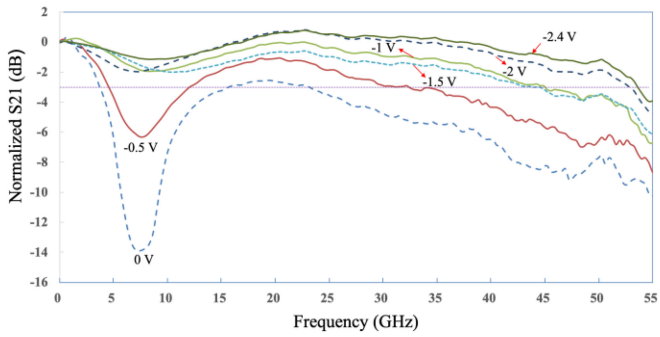

Fig. 1. A typical frequency response measured from a packaged EML by changing the bias voltage to EAM section. The termination resistance is 50 Ω and the measured 3-dB bandwidth at -2.0 V bias is 52-GHz.

Though uncooled EMLs have been reported by several groups, it is still very challenging for designing and manufacturing high-speed EMLs to meet the requirements for ultra-high-speed modulation [6], [7]. A conventional EML, which is based on the uniform grating DFB laser (UG-EML), has relatively poor resistance to residual facet reflection (RFR) that can cause output waveform distortion [8]. Such residual reflection would interfere with the laser resonance and appear as low-frequency drop (LFD) or resonant peaks in the small-signal frequency response. Fig. 1 shows an example of LFD appearing in the measured frequency response from a packaged high-speed EML. The LFD is a well-known characteristic for most high-speed EMLs and is bias-dependent since the level of RFR reaches the laser facet varies with the applied reverse bias to the modulator section. Though the laser is biased with a DC current and usually connected with a large capacitance, the reflected modulated

Manuscript received December 8, 2021; revised January 24, 2022; accepted February 4, 2022. Date of publication February 9, 2022; date of current version February 23, 2022. This work was supported by the Ministry of Science and Technology (MOST), Taiwan under Grant MOST 109-2622-E-011-001-CC1. *(Corresponding author: San-Liang Lee.)*

Siti Sulikhah, San-Liang Lee, and Lung-Wei Chung are with Electronic and Computer Engineering, National Taiwan University of Science and Technology, Taipei, ROC 106, Taiwan (e-mail: d10602812@mail.ntust.edu.tw; sllee@mail.ntust.edu.tw; d9102304@gmail.com).

Hen-Wai Tsao is with Electrical Engineering, National Taiwan University, Taipei, Taipei , Taiwan (e-mail: tsaohw@ntu.edu.tw).

Digital Object Identifier 10.1109/JPHOT.2022.3149945

This work is licensed under a Creative Commons Attribution 4.0 License. For more information, see https://creativecommons.org/licenses/by/4.0/

signals from the EAM section can still induce power fluctuation and chirp inside the laser cavity, and then affect mode stability and spectral characteristics. Signal degradation will emerge even by a tiny RFR [9], [10]. The LFD occurs at the frequency corresponding to the resonant frequency of the laser section.

The uneven modulation response at low frequency indicates that the output waveform under large-signal modulation will suffer from pattern effects, especially for long patterns of same signal levels. Besides the pattern effects, the appearance of large LFD indicates a larger RFR that can cause fluctuations in the modulated waveform. Therefore, the anti-reflection (AR) coating of the EAM output facet must have extremely low reflectivity in order to establish a desirable eye-diagram performance [11], [12]. To overcome the influence of residual reflection by optimizing the AR coating may increase the complexity in device design and fabrication. Accordingly, designing EMLs with robust characteristics may be a good strategy for low-cost and high-speed applications.

In our previous work, EMLs with partial corrugated grating type DFB laser (PCG-EML) were verified by simulation to have better single mode yield (SMY) than an UG-EML their higher immunity to the influence of RFR. There were concerns that if the performance improvement by PCG-EML can be conserved for higher data rate and its dependency on the grating length. The choice of an optimal grating length depends on the linear gain coefficient, which is crucial for attaining high signal quality and SMY [13]–[15]. We proposed here the PCG-EMLs to accomplish a smaller LFD and be relatively invulnerable to the change of RFR for transmitting ultra-high-speed signals. They will also provide better single-mode and waveform stability under the phase fluctuation of the rear facet. We verify that the PCG-EML can reduce the LFD and enlarge the eye opening for high-data-rate modulation.

II. Dependency of Low-Frequency Drop on Device Structure

The LFD arises from the interaction of the feedback time-varying photons with the carriers/photons inside the laser cavity even while the laser is biased with a DC current, so it is laser-structure dependent. In principle, this effect needs to be analyzed by taking account of the temporal and spatial dependence of the photon density and carrier density in the cavity [19]–[22]. In order to observe the effects without intensive theoretical derivations, we adopted here the simplified model developed in [23] to analyze the LFD for EMLs under the influence of RFR. The reflected modulated signal from RFR is modeled as the change in the effective front facet reflectivity, which in turn change the cavity loss of the DFB laser, α_L. By including this effect in the rate equations of DFB lasers [22], the modulation frequency response of the EAM under the RFR can be expressed as [23]:

$$\frac{P_{EAM}(\omega)}{V_1(\omega)} \propto \frac{1}{1+j\omega RC}\left(1+\frac{\kappa(j\omega+\gamma)}{\omega_R^2-\omega^2+j\omega\gamma}\right) \quad (1)$$

where ω_R and γ are the relaxation oscillation frequency and damping factor of the laser section, respectively. The modulation response of the EAM without any optical feedback is simply modeled as a low-pass filter governed by the resistance *R* and capacitance *C*. κ is a coefficient related to the optical coupling strength between the laser and EAM section as well as the change in the cavity loss due to RFR [23]:

$$\kappa \propto \Delta\alpha_L \rho e^{(-\alpha_{EAM0}L_{EAM})} \times \cos\left(2\beta_{EAM}L_{EAM}+\alpha_c\alpha_{EAM}L_{EAM}\right) \quad (2)$$

where ρ is the residual reflectivity of the AR-coated EAM facet, α_{EAM} expresses the absorption coefficient of the EAM, which is proportional to bias voltage V_1 applied to the EAM. β_{EAM} and α_c are propagation constant and chirp parameter of the EAM, respectively. $\Delta\alpha_L$ is the change in the cavity loss due to the optical feedback. Assuming a small-signal modulation to the EAM and a small RFR, the cavity loss of the laser can be written as:

$$\alpha_L = \alpha_{L0} + \Delta\alpha_L e^{j\omega t} \quad (3)$$

where α_{L0} is the cavity loss without RFR, and ω is the modulating frequency.

Equation (1) indicates clearly that the LFD occurs near the relaxation resonant frequency of the laser, which matches well with the experimental observation. It also manifests the possible appearance of a dip or peak in the frequency response, depending on the relative phase of the RFR, which is given by the propagation phase and the induced chirp in the EAM section, as given in equation (2). We add $\Delta\alpha_L$ in equation (2) from the equation in [23] to account for the dependency on DFB laser structure.

The effect of optical feedback on the laser characteristics is well-known to be dependent on the laser structure. It was proposed to address the structure dependency by expressing $\Delta\alpha_L$ as [24]

$$(\Delta\alpha_L + j\Delta\delta_L)\,L = C_L\,\Delta r_2 \quad (4)$$

where

$$\Delta r_2 = \rho C_f^2 e^{-(1+j\alpha_c)\alpha_{EAM}L_{EAM}} e^{-j\beta_{EAM}L_{EAM}} e^{j\omega t} \quad (5)$$

with Δr_2 being the change in the equivalent reflection coefficient at the laser/EAM interface of which the coupling coefficient is C_f. In equation (4), C_L is a complex coefficient, which depends only on the DFB laser modal characteristic, and $\Delta\delta_L L$ represents the phase deviation of the lasing mode.

The coefficient C_L relates the change in the cavity loss to optical feedback. It can be obtained from the lasing condition equation, or called the determinantal equation in [24], by deriving the change in the propagation constant in response to the reflectivity change Δr_2. After C_L is obtained, $\Delta\alpha_L$ can be obtained from equation (4) as

$$\Delta\alpha_L = \frac{1}{L} Re\{C_L \Delta r_2\} \quad (6)$$

Therefore, C_L determines how sensitive the optical feedback affects the laser emission frequency and threshold modal gain. It was reported in [24] that the standard UG-DFB laser could have a larger C_L than a Fabry-Perot (FP) laser with cleaved facets, so an UG-DFB laser can be more sensitive to the optical feedback than a cleaved-facet FP laser. Even a small amount of the residual reflectivity $\sim 10^{-4}$ could fluctuate the output power and signal chirp [25]. Furthermore, due to the case of DFB laser with an AR coated (emission facet), the optical fields depend on

the high-reflection (HR) facet phase and/or its grating structure [26], while the C_L of FP laser is commonly a constant that depends only on the amplitude reflectivity.

An analytic expression of $|C_L|$ is derived to relate the optical feedback sensitivity to the optical field distribution inside the laser cavity as [27]:

$$|C_L| = \frac{L_a I}{2\left|\int_0^{L_a} F(z)\, B(z)\, dz\right|} \tag{7}$$

where I is the laser output power, $F(z)$ and $B(z)$ are complex electrical amplitudes of forward and backward waves when there is no external reflection. Therefore, the laser structure that has a greater integration value of the product of forward and backward waves over the cavity will have a smaller $|C_L|$ provide that the output power is held constant. The C_L value can also be derived from the lasing condition equation, equation (5) in Ref. [28], [28], for the PCG-DFB.

From eq. (6), a larger C_L gives rise to a greater $\Delta\alpha_L$ that indicates a potentially greater LFD. Therefore, to reduce LFD for an EML requires a robust laser structure that has good immunity to optical feedback. One candidate to achieve this function is to adopt the PCG-DFB in the EAM. A PCG-DFB consists of a corrugated and a non-corrugated gain sections. In addition, it has been verified from theoretical and experimental results that the PCG-DFB lasers are less sensitive to optical feedback than a standard DFB laser [28], [29].

The simplified formulation given in equation (1) states clearly the cause of LFD by the RFR of an EML. The connection of the LFD strength with the laser structure is governed by equation (2) and (4). Roughly speaking, the laser structure that is sensitive to optical feedback suffers from a larger LFD while it is integrated with an EAM to form an EML.

Noting that the formulation of the EAM modulation response and C_L in this section is a phenomenological rather than exact approach to describe how the laser structure can affect the sensitivity of an EML by the RFR. The C_L parameter derived in Ref. [24] is based on ignoring the spatial dependency of the optical field and carrier densities along the cavity, parameter given in Ref. [24] though the final expression includes the spatial dependency of the optical field. Furthermore, for DFB lasers with HR coating on one facet, their output characteristics strongly depend on the facet phase. To fairly compare the performance of different laser structures for EMLs, it is necessary to conduct statistical analyses of the characteristics for different facet phases. Therefore, we adopt the commercial simulator to analyze the LFD and other dynamic responses rather than trying to derive lengthy formula of C_L. The simulator accounts for the spatial dependence of photon density and carrier density in the laser structure as well as different grating length ratio and facet phases.

III. Device Simulation Methodology and Parameters

Fig. 2(a) shows the cross-sectional schematic diagram of a PCG-EML, which consists of a DFB laser section of length L_a with a portion of it having a corrugated grating of length L_g and an EAM section of length L_{EAM} for RF modulation. The front

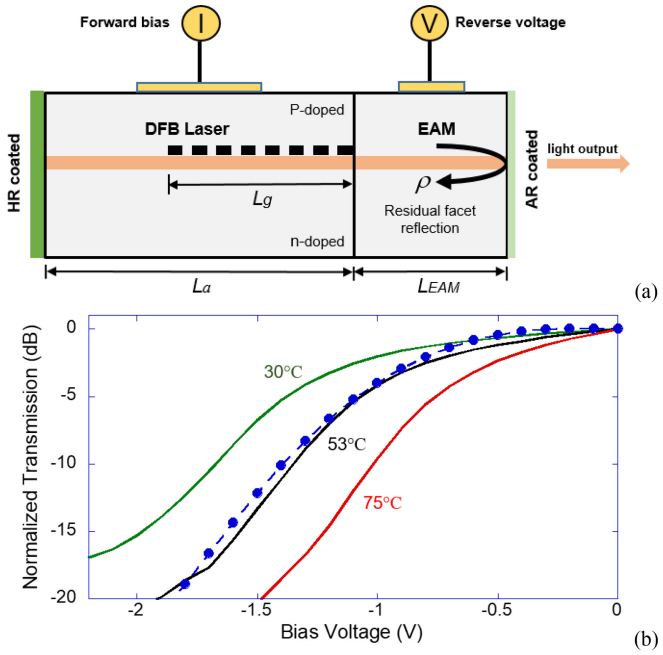

Fig. 2. (a) The cross-sectional schematic diagram of EML with partially corrugated grating. (b) Measured EAM absorption curve and the curve fitting for modeling. Solid and dashed lines are measured and simulated curves, respectively.

and rear sections are separated by an isolation region. The rear facet (laser end) is coated with HR film of 90% reflectivity, while the front facet (EML output end) is AR coated with some residual reflection due to imperfect AR coating. When the grating ratio, which is defined as $\rho_r = L_g/L_a$, is equal to 1, the device becomes a conventional UG-DFB based EML, referred as UG-EML hereafter [16]–[18].

The device modeling of EMLs is conducted by using the time-dependent Transmission Line Laser Model (TLLM) of the VPIcomponentMaker Photonics Circuits Tool, which has been applied to analyze many circuits and optoelectronic devices, e.g., DFB laser, FP laser, passive feedback laser, hybrid integrated semiconductor laser, optically injected laser, and complex photonic integrated structures like EMLs [30]–[35]. The TLLM simulation model can account for the spatial dependency of the carrier density as well as the forward and backward propagating waves inside the laser by dividing the device into multiple longitudinal sections [36], [37]. This model includes the optical and electronic interactions, e.g., scattering of light, among different device sections. In addition, the facet reflections are also included in the simulation model. The photo-carrier and photon-photon interactions under optical feedback fluctuate the spectral and temporal characteristics of the DFB laser section and deviate the wavelength.

The values of the key device parameters used in analyzing static and dynamic performances of EMLs are summarized in Table I. The laser gain material involves a typical MQW structure operating at 1310-nm wavelength. The DFB laser has a threshold current of 13 mA, and it is biased with a DC current of 70 mA. The normalized transmission curve (dashed line) of the EAM

TABLE I
LIST OF DEVICE PARAMETERS

Parameter	Value	Unit
DFB section length	300	μm
Active region width	1.8	μm
Active region depth of MQW	0.03	μm
Confinement factor of MQW	0.075	-
Grating coupling strength, κ	5000	m^{-1}
Gain compression factor	$2.5x10^{-23}$	m^3
Internal loss	25	cm^{-1}
Group index	3.73	-
Injection efficiency	0.75	-
Transparent carrier density	1.5×10^{24}	$1/m^3$
Linewidth enhancement factor	3	-
Gain Model of EAM		
Shape	Lorentzian	-
EAM length	100	μm
Peak absorption	$1.1x10^5$	1/m
Peak absorption linear	$5.4x10^5$	1/Vm
Peak absorption quadratic	$1.51x10^6$	$1/V^2m$
Peak absorption cubic	$4.4x10^5$	$1/V^3m$
Peak absorption frequency	234.025	THz
Peak absorption frequency linear	2.12	THz
Absorption bandwidth	3.82	THz
Absorption bandwidth linear	-2.56	THz/V
Saturation carrier density	$5x10^{24}$	$1/m^3$

is obtained from the measured EML absorption at 30°C, 53°C, and 75°C, as depicted in Fig. 2(b).

Before investigating LFD and other dynamic characteristics with the simulation tool, the material and device parameters are adjusted for matching with the measured static characteristics of EMLs, including threshold current, extinction ratio (ER), and side-mode suppression ratio (SMSR). Then, the single-mode yield (SMY) and eye diagrams for NRZ or PAM-4 modulation under the influence of HR facet phase variations and RFR [38], [39] will be analyzed. The statistics of the simulated device performance is evaluated by varying the rear facet phase from 0 to 2π to account for the HR facet phase fluctuation caused by device cleavage. The SMY is specified as the percentage of phase that the laser can have >35-dB dynamic SMSR, assuming the phase fluctuation is uniformly distributed between 0 and 2π. Moreover, the Q-value that determines the signal-to-noise ratio of the output waveform is calculated. The average Q-value for a given EML condition is obtained by averaging the calculated Q over the HR facet phase range having >35-dB SMSR, which represents the device performance after screening out devices with poor single-mode performance. Note that only the dynamic responses of the EMLs with good SMSR are measured for comparisons with the experimental results where only good devices were bonded on the carriers for these measurements.

IV. EXPERIMENTAL RESULTS

EMLs of different grating ratios were fabricated based on the design aiming for 56-Gbaud/s operation in the 1310-nm wavelength. The EMLs were outsourcing to an InP-based semiconductor manufacturer for production and measurements. The lasers and modulators were designed with different quaternary

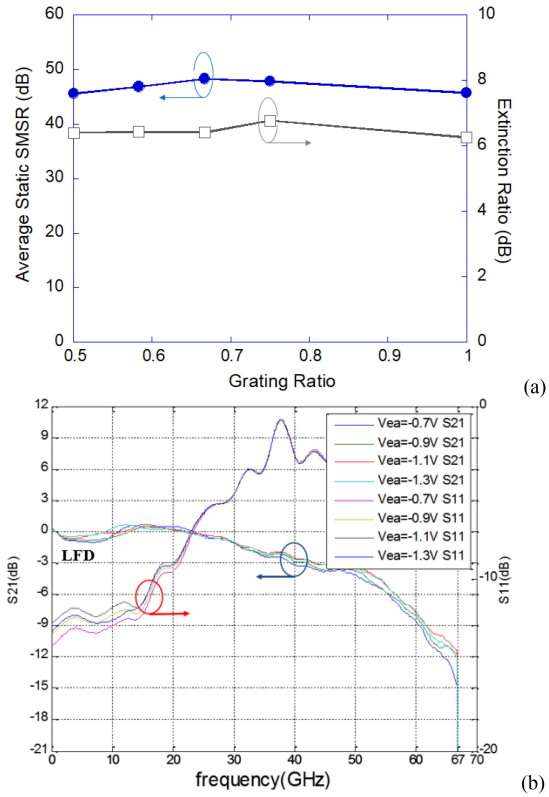

Fig. 3. (a) Average static SMSR and ER for PCG-EMLs of different grating ratios. (b) Normalized S-parameters for PCG-EMLs ($\rho_r = 0.66$).

MQW structures on InP substrate. The laser and EAM sections were fabricated with wet etching and butt-joint epitaxial regrowth using metal organic chemical vapor deposition (MOCVD) epitaxy. The laser and EAM sections are 300-μm and 100-μm long, respectively. The gratings for DFB lasers were patterned with holographic exposure. The EML was fabricated into 1.8-μm wide ridge waveguide structure with high-speed designs of metal pads and dielectric layers. The facet reflectivity of AR coating was estimated to be 10^{-3} or smaller. After screening out devices with out-of-spec DC characteristics, the devices were bonded on the high-speed carriers for high-speed test. Due to the limitation of equipment, the eye-diagrams were measured with 28-Gb/s PRBS NRZ signals, while the S-parameters were measured up to 67-GHz to verify the device bandwidth.

The static SMSR of the EMLs is typically >45 dB for all structures, as shown in Fig. 3(a). The typical absorption curves of the EAM section are depicted in Fig. 2(b) where >6-dB extinction ratio (ER) can be obtained with 0.5 V modulation voltage, as shown in Fig. 3(a). There is no clear difference in the static SMSR and ER among EMLs of different grating ratios. Fig. 3(b) depicts an example of measured S-parameters for PCG-EMLs with various bias voltages. The EMLs can have 3-dB modulation bandwidth of >40-GHz. Since all EMLs have the same EAM section, the modulation bandwidth is similar for PCG- and UG-EMLs, as shown in Fig. 4(a). In the S21 curves, a shallow low-frequency drop occurs at about 5-GHz, which corresponds to the relaxation resonance (f_r) of the DC-biased DFB laser.

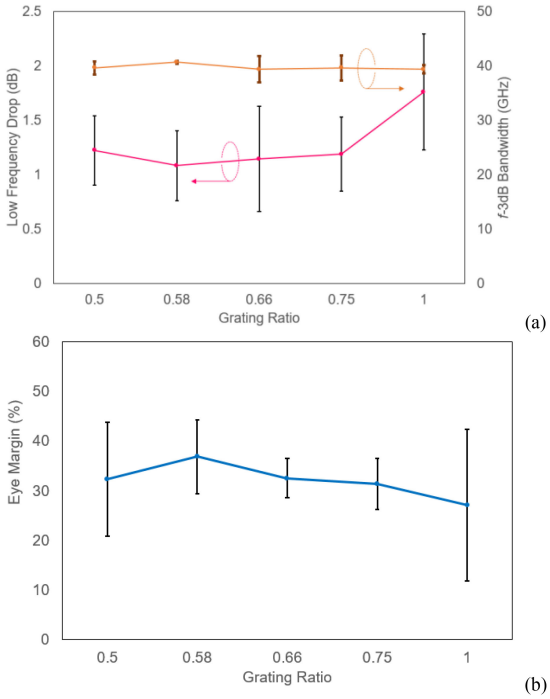

Fig. 4. (a) Measured LFD and *f*-3dB bandwidth of EMLs. (b) Eye margin for EMLs of different grating ratios.

Fig. 4(a) also depicts the measured LFD for EMLs with different grating ratios. The LFD is defined as the dip in the S21 curve around f_r when the EAM is biased at -1 V bias. This LFD can reveal the relative influence of the RFR on the EML dynamics since it is caused by the induced-fluctuation on the carrier density of a DC-biased laser from the optical modulation of the residual reflection on the modulator. The induced-fluctuation reaches the maximum at f_r. The results verify that PCG-EMLs can have smaller average magnitude and smaller fluctuation of LFD than the UG-EML has. That is, the difference in LFD between the PCG-EMLs and UG-EML is clear, so a conventional UG-EML can be strongly affected by the RFR and degrade the signal quality. Among the PCG-EMLs of different grating ratios, there is no clear difference in the measured LFD though the grating ratio around 0.6 seems to have the best LFD performance.

To justify the performance enhancement, the measured eye margin for EMLs with different grating ratios is depicted in Fig. 4(b), which is extracted from measured eye diagrams under 28-Gb/s NRZ modulation. As expected, the PCG-EMLs provides a better average eye margin (36.83%) than UG-EML ($\sim$27%) since the latter is relatively sensitive to reflection effects. It also shows that the best eye margin could be achieved when the grating ratio is about 0.6.

V. Simulation Results and Discussion

A. Dynamic Performance of EMLs Under 56-Gb/s NRZ Signal Modulation

The analysis with aforementioned simulation tool is conducted to evaluate the feasibility EMLs in high-data-rate transmission as well as to investigate the influence of LFD.

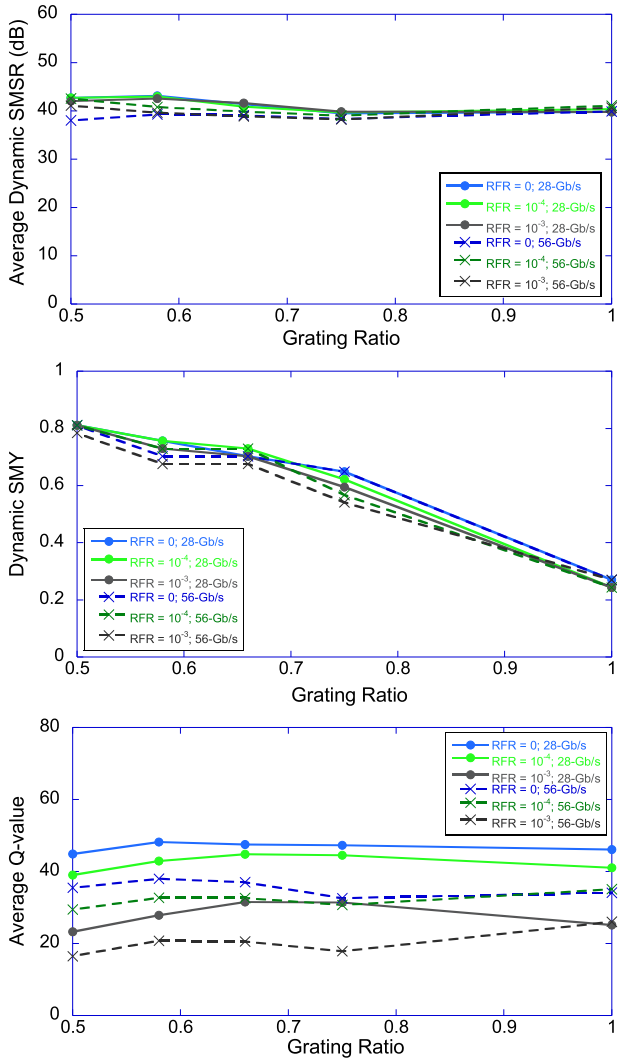

Fig. 5. The average dynamic SMSR (top), dynamic SMY (middle), and average Q-value (bottom) for EMLs of different RFRs under 28-Gb/s and 56-Gb/s NRZ.

The simulation is performed with device parameters of L_a = 300-μm and L_{EAM} = 100-μm. The waveform quality is analyzed by transmitting $2^{21}-1$ pseudorandom bit sequence (PRBS) data stream with a transmitter LPF bandwidth of 75% data rate [22], [40]. For the simulation of dynamic response, the EAM is modulated by 56-Gb/s PRBS-NRZ pattern and/or up to 112-Gbaud/s PAM-4 signal with 0.5 V voltage swing and a reverse bias voltage of -1 V. A 5$^{\text{th}}$-order low pass filter (LPF) is set at transmitter side to smooth out the modulation signal and reduce the signal overshoot/undershoot. Fig. 5 shows the average dynamic SMSR, dynamic SMY, and average Q-value for EMLs of different RFRs under 28-Gb/s (solid line) and 56-Gb/s NRZ modulation (dashed line), respectively. The most significant difference between PCG-EMLs and UG-EMLs ($\rho_r = 1$) happens for the dynamic SMY. The PCG-EML can obtain >80% of dynamic single-mode yield, which is much better than the UG-EML (<27.03%). The UG-EML is relatively sensitive to the change in HR facet phase of the laser section,

which can be easily perturbed by the fluctuation in carrier and photon densities by the RFR.

There is no clear difference in dynamic SMSR and Q-value between PCG-EMLs and UG-EMLs after screening out the poor static-SMSR devices. The RFR can increase or decrease the quality factor of the output waveform generated by an EML, depending on the phase relationship of the RFR and laser resonance. For RFR values varying from 0 to 10^{-3}, the average Q-value degrades significantly. In overall, PCG-EMLs with a grating ratio of around 0.6 seems to be the optimal condition since it maintains an excellent single-mode yield and average Q-value under the influence of RFR at a higher data rate operation.

Fig. 6 shows the real-time longitudinal power distribution for PCG-EML under 56-Gb/s NRZ signal modulation with $L_g = 225$-μm (Fig. 6(a)) and UG-EML (Fig. 6(b)) under 10^{-3} RFR and 0.9 HR facet reflectivity where different curves correspond to the light power distribution at different time instances. The phase of HR facet was set to 300° for both cases. The results certify the stable operation of a PCG-EML, while the UG-EML suffers from larger fluctuation in the field distribution caused by RFR. Due to the nearly flat power distribution in the FP section of a PCG-EML, the immunity to RFR is greatly improved for PCG-EML. Thus, a PCG-EML could produce much clear eye opening than an UG-EML for a facet reflectivity as large as 10^{-3}, which can be clearly observed in Fig. 6(c) and (d).

B. Low-Frequency Drop

Fig. 7(a) displays the simulated LFD for EMLs with different RFRs and grating ratios. Again, the statistics is obtained by varying the HR facet phase and screening out the phases with poor SMSR. Overall, the PCG-EMLs with a grating ratio around 0.6 could give smaller average LFD of 0.395, 0.647, and 1.44 for 10^{-4}, 10^{-3}, and 10^{-2}, respectively. The improved immunity to residual facet reflection for PCG-EMLs results from the insensitivity to the relative phase between the HR facets and the gratings. The relative phase between HR facet and gratings greatly affect the output waveform since it is sensitive to the optical feedback induced fluctuation in field and carrier distributions. On other hand, UG-EMLs ($\rho_r = 1$) have a larger average LFD due to their relatively poor resistance to RFR, which strongly disturbs the non-uniform longitudinal power distribution, as shown in Fig. 6(d). The PCG-DFB based EMLs, where the laser section can be considered as a FP-laser cavity formed by the HR facet and an active grating mirror, can have stable longitudinal power distribution under the influence of RFR. The simulation reveals the similar trend of LFD-vs-grating ratio as the measured results, as shown in Fig. 4(a), and the optimal grating ratio is 0.66 by simulation and 0.58 by experiments.

The RFR-induced LFD is expected to deteriorate the signal quality of high-speed modulation by the EML. The Q-value of the output waveform from EMLs of different LFDs is shown in Fig. 7(b) for 56-Gb/s NRZ modulation. Different LFD values were obtained from EMLs of different grating ratios and different facet phases that produce the data in Fig. 7(a). The Q-value can be kept above 20 for LFD = 1 dB and worsened

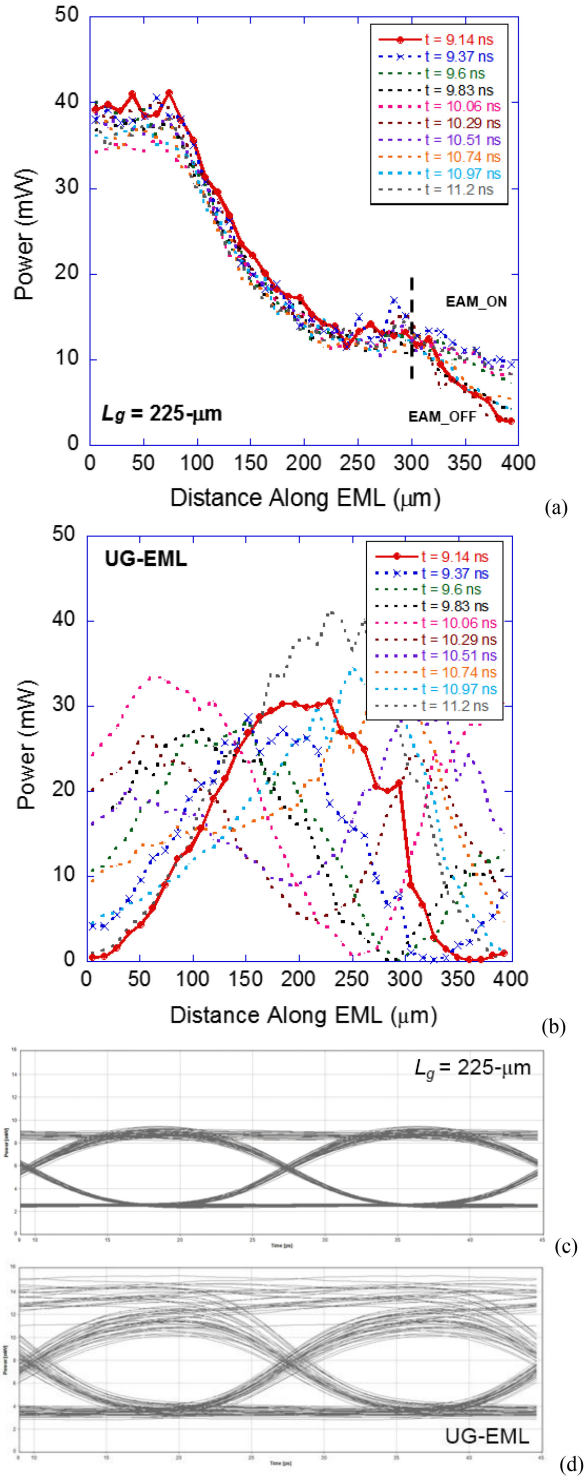

Fig. 6. Real time total longitudinal power distribution for (a) $L_g = 225$-μm, (b) UG-EML and eye diagrams under 56-Gb/s NRZ modulation with 10^{-3} RFR for (c) $L_g = 225$-μm, and (d) UG-EML. HR facet phase is set by 300°.

for larger LFD. The degradation in the waveform quality can be even more severe when multi-level modulation formats are employed. As stated before, the LFD can indicate the effect of RFR on an EML, it can be one of the key performance indices for qualifying the EMLs for high-capacity data transmission. That

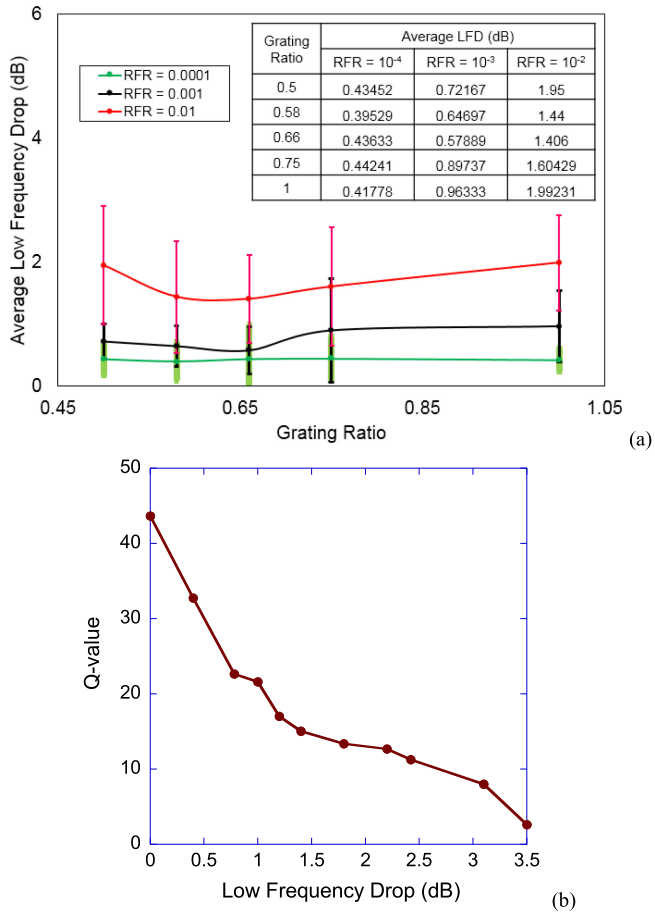

Grating Ratio	Average LFD (dB)		
	RFR = 10^{-4}	RFR = 10^{-3}	RFR = 10^{-2}
0.5	0.43452	0.72167	1.95
0.58	0.39529	0.64697	1.44
0.66	0.43633	0.57889	1.406
0.75	0.44241	0.89737	1.60429
1	0.41778	0.96333	1.99231

Fig. 7. (a) Simulated LFD for EMLs with different RFRs and grating ratios, and (b) Q-value for EMLs of different LFDs for modulation with 56-Gb/s NRZ.

is, the EMLs with large LFD at the operation bias condition have better to be screened out because of potential poor modulation signal quality.

C. Modulated Waveform Analyses for EMLs Under 56-Gbaud/s and Beyond PAM-4 Signal

The influence of LFD may be more critical for PAM-4 modulation. As undershoot and overshoot arises during signal waveform transition, the RFR could lead to severe degradation on eye-openings for PAM-4 modulation, especially for the EMLs with larger LFD.

Fig. 8 compares the PAM-4 modulated waveforms for EMLs of different LFDs between 56-Gbaud/s and 112-Gbaud/s. In the simulation, the EMLs under 56-Gbaud/s and 112-Gbaud/s modulation are assumed to have 42-GHz and 65-GHz 3-dB bandwidth, respectively, by adding a LPF of the corresponding bandwidth at the transmitter side. As expected, the EML with a small LFD can produce a better eye-opening due to the stable laser operation under the influence of RFR. In contrast, the EML with a larger LFD encounters a more severe fluctuation of carrier density and photon density in the laser section, which in turn distorts the output waveform as the fluctuated laser light passes through the EAM section.

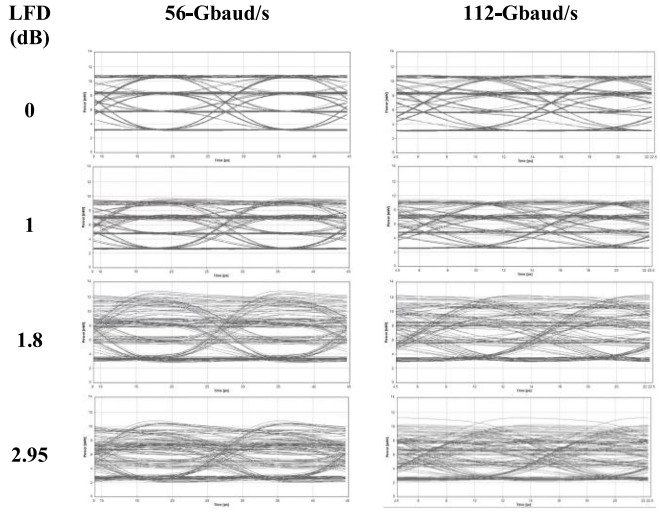

Fig. 8. PAM-4 modulated waveform for EMLs of different LFDs. Bandwidth of LPF filter is 42-GHz and 65-GHz at 56-Gbaud/s and 112-Gbaud/s PAM-4 signals, respectively.

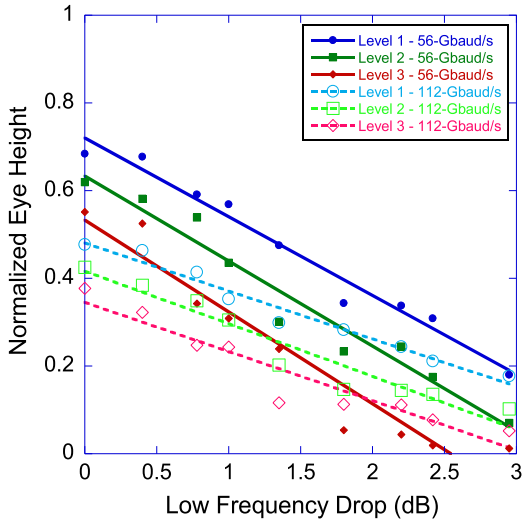

Fig. 9. Normalized eye height for EMLs of different LFDs under 56-Gbaud/s and 112-Gbaud/s PAM-4 modulation.

Fig. 9 summarizes the normalized eye height for the three eye openings of a PAM-4 signal for EMLs of different LFD values. The EMLs with a larger LFD will suffer from more waveform fluctuation caused by the RFR. The normalized eye height is smaller for the 112-Gbaud/s modulation due to the assumed smaller percentage of bandwidth over data rate for practical implementation. The smaller percentage of bandwidth tends to suppress the overshoot and undershoot caused by the RFR, so the normalized eye height drops slower for 112-Gbaud/s than the 56-Gbaud/s case. Thus, there may exist a trade-off in choosing the optimal bandwidth for an EML if the LFD can not be eliminated. The LFD can be suppressed by enhancing the AR coating and/or reducing the reflection by adding a tilted waveguide or window structure of EML front facet [41], [42]. It can also be suppressed by adopting a laser structure, like PCG-DFB, to have better immunity to the RFR.

VI. Conclusion

We have successfully evaluated the performance of EMLs under the influence of residual facet reflection by both experiments and simulations with an emphasis on the resultant low-frequency drop. The LFD can be a clear indicator for how the RFR affects the performance of an EML. It is not only related to the value of RFR but also the immunity to optical feedback influence for the laser structure in an EML. Both experimental and simulation results show that the EMLs based on PCG-DFB laser structure can have smaller LFD and better resistance to RFR. The optimal grating ratio of $\sim$0.6 is obtained for the PCG structure to have small LFD.

The most significant difference between a PCG-EML and UG-EML is the dynamic single-mode yield under the influence of RFR. For a PCG-EML, high dynamic SMY of $>$80% can be obtained even under 10^{-3} RFR, while the UG-EML has only 27% SMY under the same value of RFR. After screening out the devices with poor SMSR, the average LFD and Q-value show less significant difference between these two types of EMLs. However, the PCG-EML still provide smaller LFD and larger average Q-value than the UG-EML. The smallest average LFD under 10^{-3} RFR is 0.58 for $\rho_r = 0.66$, while the optimal grating ratio in terms of LFD occurs at $\rho_r = 0.58$ for an unknown RFR (estimated to be 10^{-3}) from the experimental data.

Though the LFD appears at the relatively low frequency position of the small-signal modulation response for an EML with $>$40GHz bandwidth, it has strong effect on the output waveform when the EML is under high data-rate modulation. The low-frequency dip (or peak) in the modulation response is expected to cause concerns when the modulation data consist of long-stream of "0" or "1" bits. In addition, it indicates the severity of RFR effects on the overshoot and undershoot of modulated waveform. The overshoot and undershoot can cause severe signal degradation for multi-level modulation format. The simulation of output waveforms for 56-Gbaud/s and 112-Gbaud/s PAM-4 modulation shows the rapid decrease in eye opening as the LFD increases. Therefore, the LFD can be a key performance indicator to screen out the EMLs that are very likely to be affected by RFR.

Acknowledgment

The authors would like to thank Che-Jen Chang, Dawei Ren, Emin Chou, and Yu-Heng Jan of Source Photonics Inc. for the help on this work.

References

[1] J. D. Ambrosia, "The case for 1.6 terabit ethernet," in *Proc. IEEE 802.3 Beyond 400 Gb/s Ethernet Study Group Meeting*, 2021, pp. 1–18.

[2] O. Ozolins *et al.*, "100 GHz externally modulated laser for optical interconnects," *J. Lightw. Technol.*, vol. 35, no. 6, pp. 1174–1179, Jan. 2017.

[3] Y. Cheng, Q. J. Wang, and J. Pan, "1.55 μm high speed low chirp electroabsortion modulated laser arrays based on SAG scheme," *Opt. Exp.*, vol. 22, no. 25, pp. 31286–31292, Dec. 2014.

[4] C. Lam, X. Zhou, and H. Liu, "200G per lane for beyond 400GbE," in *Proc. IEEE 802.3 NEA Meeting*, 2020, pp. 1–20.

[5] K. Naoe, T. Nakajima, Y. Nakai, Y. Yamaguchi. Y. Sakuma, and N. Sasada, "Advanced InP laser technologies for 400G and beyond hyperscale interconnections," in *Proc. SPIE Photon. Eur. Conf.*, 2020, Art. no. 1135604.

[6] J. J. S. Huang *et al.*, "Manufacturing excellence and future challenges of wireless laser componets for 4G/5G optical mobile fronthaul networks," in *Proc. 27th Wireless Optical. Commun. Conf.*, 2018, pp. 1–2.

[7] W. Kobayashi *et al.*, "Design and fabrication of 10-/40-Gb/s, uncooled electroabsorption modulator integrated DFB laser with butt-joint structure," *J. Lightw. Technol.*, vol. 28, no. 1, pp. 164–171, Jan. 2010.

[8] M. Yamaguchi, T. Kato, T. Sasaki, K. Komatsu, and M. Kitamura, "Requirements for modulator-integrated DFB LD's for penalty-free 2.5-Gb/s transmission," *J. Lightw. Technol.*, vol. 13, no. 10, pp. 1948–1954, Oct. 1995.

[9] H. G. Shiraz, *Distributed Feedback Laser Diodes and Optical Tunable Filters*. Southern Gate, Chichester, England: Wiley, 2003.

[10] O. K. Kwon, Y. S. Baek, and Y. C. Chung, "Electroabsorption modulated laser with high immunity to residual facet reflection," *IEEE J. Quantum Electron.*, vol. 48, no. 9, pp. 1203–1213, Sep. 2012.

[11] M. Aoki, S. Takashima, Fujiwara Y, and S. Aoki, "New transmission simulation of EA-moudator integrated DFB-lasers considering the facet reflection-induced chirp," *IEEE Photon. Technol. Lett.*, vol. 9, no. 3, pp. 380–382, Mar. 1997.

[12] C. Sun *et al.*, "Influence of residual facet reflection on the eye-diagram performance of high-speed electroabsorption modulated lasers," *J. Lightw. Technol.*, vol. 27, no. 15, pp. 2970–2976, Aug. 2009.

[13] P. D. Pukhrambam, S. L. Lee, and G. Keiser, "Electroabsorption modulated lasers with immunity to residual facet reflection by using lasers with partially corrugated gratings," *IEEE Photon. J.*, vol. 9, no. 2, Apr. 2017, Art. no. 7101016.

[14] P. D. Pukhrambam and S. L. Lee, "Highly residual facet reflection immune electro-absorption modulated laser with short partially corrugated gratings," in *Proc. Int. Semicond. Laser Conf.*, 2016, pp. 1–2.

[15] S. Sulikhah *et al.*, "Demonstration of improved immunity to residual facet reflection for uncooled EMLs with partially corrugated grating," in *Proc. Opto-Electron. Commun. Conf.*, 2020, pp. 1–3.

[16] J. J. S. Huang, Y. H. Jan, D. Ren, Y. C. Hsu, P. Sung, and E. Chou, "Defect diffusion model of InGaAs/InP semiconductor laser degradation," *Appl. Phys. Res.*, vol. 8, no. 1, pp. 149–157, Jan. 2016.

[17] J. J. S. Huang, Y. H. Jan, J. Chang, Y. C. Hsu, D. Ren, and E. Chou, "Swift reliability test methodology of 100G high-speed, energy-efficient electro-absorption modulated lasers (EML) for green datacenter networks," *RedFame*, vol. 3, no. 1, pp. 74–80, Aug. 2016.

[18] J. J. S. Huang *et al.*, "ESD polarity effect study of monolithic, integrated DFB-EAM EML for 100/400G optical networks," in *Proc. Conf. Lasers Electro-Opt. Pacific Rim*, 2017, pp. 1–4.

[19] R. A. Salvatore, R. T. Sahara, M. A. Bock, and I. Libenzon, "Electroabsorption modulated laser for long transmission spans," *IEEE J. Quantum Electron.*, vol. 38, no. 5, pp. 464–476, May 2002.

[20] P. Brosson and H. Bissessur, "Analytical expressions for the FM and AM responses of an integrated laser-modulator," *IEEE J. Sel. Topics Quantum Electron.*, vol. 2, no. 2, pp. 336–340, Jun. 1996.

[21] B. Tromborg, H. Olesen, X. Pan, and S. Saito, "Transmission line description of optical feedback and injection locking for Fabry-Perot and DFB lasers," *IEEE J. Quantum Electron.*, vol. QE-23, no. 11, pp. 1875–1889, Nov. 1987.

[22] L. A. Coldren, S. W. Corzine, and M. L. Masanovic, *Diode Laser and Photonic Integrated Circuits*, 2nd ed. Hoboken, NJ, USA: Wiley, 2012.

[23] C. Sun *et al.*, "Fabrication and packaging of 40-Gb/s AlGaInAs multiple-quantum-well electroabsorption modulated lasers based on identical epitaxial layer scheme," *J. Lightw. Technol.*, vol. 26, no. 11, pp. 1464–1471, Jun. 2008.

[24] F. Favre, "Theoretical analysis of external optical feedback on DFB semiconductor lasers," *IEEE J. Quantum Electron.*, vol. 23, no. 1, pp. 81–88, Jan. 1987.

[25] I. P. Kaminow, G. Eisenstein, and L. W. Stulz, "Measurement of the modal reflectivity of an antireflection coating on a superluminescent diode," *IEEE J. Quantum Electron.*, vol. QE-19, no. 4, pp. 493–495, Apr. 1983.

[26] F. Grillot, B. Thedrez, and G. H. Duan, "Feedback sensitivity and coherence collapse threshold of semiconductor DFB lasers with complex structure," *IEEE J. Quantum Electron.*, vol. 40, no. 3, pp. 231–240, Mar. 2004.

[27] T. Hirono, T. Kurosaki, and M. Fukuda, "A novel analytical expression of sensitivity to external optical feedback for DFB semiconductor lasers," *IEEE J. Sel. Topics Quantum Electron*, vol. 28. no. 12, pp. 2674–2677, Dec. 1992.

[28] Y. Huang, T. Okuda, K. Shiba, and T. Torikai, "High-yield external optical feedback resistant partially corrugated waveguide laser diodes," *IEEE J. Sel. Topics Quantum Electron.*, vol. 5, no. 3, pp. 435–441, May/Jun. 1999.

[29] Y. Huang, T. Okuda, K. Shiba, Y. Muroya, N. Suzuki, and K. Kobayashi, "External optical feedback resistant 2,5-Gb/s transmission of partially corrugated waveguide laser diodes over a −40°C to 80°C temperature range," *IEEE Photon. Technol. Lett.*, vol. 11, no. 11, pp. 1482–1484, Nov. 1999.

[30] V. Photonics, "VPI component maker photonic circuit," Accessed: Feb. 11, 2022. [Online]. Available: https://www.vpiphotonics.com/Tools/PhotonicCircuits/.

[31] S. Sulikhah, S. L. Lee, and H. W. Tsao, "Improvement on direct modulation responses and stability by partially corrugated gratings based DFB lasers with passive feedback," *IEEE Photon. J.*, vol. 13, no. 1, Apr. 2021, Art. no. 4900214.

[32] Y. Li *et al.*, "Optical comb generator with flat-topped spectral response using one electroabsorption-modulated laser and one phase modulator," *Opt. Eng.*, vol. 59, no. 1, Jan. 2020, Art. no. 016112.

[33] J. Declercq *et al.*, "Low power all-digital radio-over-fiber transmission for 28-GHz band using parallel electro-absorption modulators," *J. Lightw. Technol.*, vol. 39, no. 4, pp. 1125–1131, Oct. 2020.

[34] Y. Bao *et al.*, "50Gbps DDO-OFDM transmission after 80km without DCF based on an electro-absorption modulator," in *Proc. 10th Int. Conf. Opt. Commun. Netw.*, 2011, pp. 1–2.

[35] I. Koltchanov, A. Richter, E. Myslivets, and C. Kazmierski, "Complete time and frequency-dependent modeling of electro-absorption modulators," in *Proc. OFC/NFOEC Tech. Dig.. Opt. Fiber Commun. Conf.*, 2005, Art. no. OME42.

[36] A. Lowery *et al.*, "Multiple signal representation simulation of photonic devices, systems, and networks," *IEEE J. Sel. Topics Quantum Electron.*, vol. 6, no. 2, pp. 282–296, Mar./Apr. 2000.

[37] A. J. Lowery, "New dynamic multimode model for external cavity semiconductor lasers," *IEE Proc. J. Optoelectron.*, vol. 136, no. 4, pp. 229–237, Aug. 1989.

[38] O. Ozolins *et al.*, "100 Gbaud 4PAM link for high speed optical interconnects," in *Proc. Eur. Conf. Opt. Commun.*, 2017, pp. 1–3.

[39] E. E. Fiky, M. Chagnon, M. Sowailem, A. Samani, M. M. Osman, and D. V. Plant, "168-Gb/s single carrier PAM4 transmission for intra-data center optical interconnects," *IEEE Photon. Technol. Lett.*, vol. 29, no. 3, pp. 314–317, Feb. 2017.

[40] F. Chang, *Datacenter Connectivity Technologies: Principles and Practice*. Gistrup, Denmark: River Publishers, 2017.

[41] J. S. Choe, Y. H. Kwon, J. S. Sim, and S. B. Kim, "40 Gbps electroabsorption modulated DFB laser with tilted facet formed by dry etching," *Semicond. Sci. Technol.*, vol. 22, no. 7, pp. 802–805, Jul. 2007.

[42] B. H. Park *et al.*, "Investigation of optical feedback in high speed electroabsorption modulated lasers with window region," *IEEE Photon. Technol. Lett.*, vol. 17, no. 4, pp. 777–779, Apr. 2005.